Journal of Bio- and Tribo-Corrosion (2019) 5:19
https://doi.org/10.1007/s40735-018-0211-7

# Influence of White Aluminum Dross on the Corrosion Resistance of Reinforcement Carbon Steel in Simulated Concrete Pore Solution

**Roland Tolulope Loto**[1] · **Ayobami Busari**[2]

Received: 9 July 2018 / Revised: 7 December 2018 / Accepted: 11 December 2018 / Published online: 19 December 2018


**Abstract**
Recent research in concrete technology now focuses on partial replacement of cement using cost-effective, eco-friendly and sustainable wastes and admixtures. The effect of white aluminum dross (Al-D) at 0%, 5%, 10%, 15%, 20% and 25% weight concentration on the corrosion resistance of low carbon steel in simulated concrete pore solution was studied with potentiodynamic polarization technique and open circuit potential (OCP) measurement. Optical microscopy was used to analyze and compare the surface morphology of the steel specimens before and after the corrosion test. Results from electrochemical test showed Al-D in concrete admixture mildly increases the corrosion rate of the carbon steel with respect to Al-D concentration. Corrosion rate values of $3.00\times10^{2}$, $3.41\times10^{2}$ and $8.39\times10^{2}$ were obtained at 0%, 5% and 25% Al-D. Cathodic shift in corrosion potential was observed due to selective deterioration of the steel. However, potentiostatic data show the presence of Al-D extends the passivation range of the carbon steel, improving its pitting corrosion. OCP plots with and without shift significantly to positive values with respect to exposure time signifying formation of protective oxide on the carbon steel. Severe morphological deterioration in the form of corrosion pits are visible on steel surface from concrete pore electrolyte at 0% Al-D. Fewer and comparatively smaller corrosion pits are visible on the morphology of the steel from 5% Al-D pore electrolyte. The relative size of the corrosion pits decreased further from observation of the steel from pore solution at 25% Al-D.

**Keywords** Corrosion · Concrete · Pitting · Steel · Aluminum

## 1 Introduction

Concrete is a composite material consisting of coarse and fine granular aggregates contained in a hard matrix of binders. Reinforced concrete is extensively used for building and construction. The reinforcements give higher tensile strength to the concrete, but their relatively weak resistance to corrosion endangers the durability of the concrete structure. Deterioration of concrete frameworks and infrastructures due to reinforcement corrosion is a problematic phenomenon worldwide resulting in huge damage, safety issues, economic loss, and enormous repair and replacements costs [1–5]. There are several methods in place to increase the life span of reinforced concrete structures such as cathodic protection, high chromium steel, corrosion inhibitors, rebar coatings, re-alkalization, high performance concrete etc. [6, 10]. The demand for novel techniques to reduce the rate reinforced material corrosion in concrete cannot be over emphasized as there are currently limited cost-effective and economical techniques available [11–13]. Reinforcing steel in concrete is usually shielded from corrosion because of the formation of a protective oxy-hydroxide on the steel in the presence of adequate $O_2$ which passivates its surface when the alkalinity (pH 12.5–13.5) of the concrete pore solution is high [14–16]. Several factors are responsible for the formation of protective oxide, e.g., type of aggregates, temperature, humidity, moisture content, etc. [17, 18]. Basically, there are two ways by which the protective oxy-hydroxide layer of carbon steel reinforcement can be destroyed. (a) Accumulation of chloride anions close to the reinforcing steel. This is due to ingress of chloride anions from mixture of concrete impurities with moisture through pores, holes and cracks within the concrete which eventually leads to competitive adsorption

✉ Roland Tolulope Loto
tolu.loto@gmail.com

[1] Department of Mechanical Engineering, Covenant University, Ota, Ogun State, Nigeria

[2] Department of Civil Engineering, Covenant University, Ota, Ogun State, Nigeria

with $OH^-$ on the oxide surface [19]. (b) Decrease in concrete pH due to dilution of concrete pore solution by $CO_2$ from the atmosphere resulting in carbonation whereby the numbers of defects in passive layer on rebar increase [20–22]. The corrosion products from the processes mentioned above increase the pressure within the concrete, creating more cracks, causing pitting of the reinforced steel and expansion of the rust layer. These eventually weaken the concrete structure [23, 24]. Currently, carbon steel is still the dominant rebar in concrete structures. Carbon steel passivates in concrete due to incidental electrochemical reduction reaction between the steel surface and alkaline concrete pore solution [25]. Previous researches on the electrochemical behavior of carbon steel in concrete pore solution and the nature and the composition of the passive film conclude that the passivity of the steel is influenced by their chemical compositions and solution environment [26–29]. Research on concrete pore solution is important because of the mobility of trace elements which accounts for ion exchange of concrete in the hardened state. In the pursuit of cost-effective, sustainable and eco-friendly concrete, recent research in concrete technology now focuses on partial replacement of cement using some sustainable admixtures and wastes such as aluminum dross (Al-D). Al-D obtained from aluminum smelting process can be non-salt containing (white dross) or salt containing (black dross) [30–32]. Million tons of these waste is generated daily. The reuse of this material is important in a bid to reduce solid waste and promote trash to treasure initiative in line with sustainable development goals. Busari et al. [33] assessed the utilization of Al-D as a stabilizer in road construction for the improvement of pavement interlayer properties. The use of this material in concrete production both as a filler, aggregate replacement and cement replacement has been assessed by several authors [34–37]. Results showed the material proved to be a good and sustainable material in concrete production. However, the dearth of literature exists on the effect of this material on the corrosion of reinforcing steel in concrete. In view of the above, this research aims to study the influence of non-salt containing Al-D in simulated concrete pore solution on the corrosion resistance and active–passive behavior carbon steel bars.

## 2 Experimental Methods

### 2.1 Material

Low carbon steel rods were purchased from the open market in Lagos, Nigeria, and analyzed with Phenom proX scanning electron microscope (Model No. MVE0224651193) at the Materials Characterization Laboratory, Department of Mechanical Engineering, Covenant University, gave the nominal wt% composition in Table 1. The steel rods were cut and sectioned to average dimensions of 1.1 cm by 1.15 cm (length by diameter). They were subsequently grinded with silicon carbide abrasive papers (grits of 120, 220, 320, 600, 800 and 1000) and polished to 6 µm with diamond polishing paste. Portland lime stone cement conforming to NIS 444-1:2003 [38] standard was the cement used in the research; in addition, fine aggregate conforming to NIS 13:1974 [39] obtained from Ota, Ogun State, Nigeria, was also used. Portable $H_2O$ was used in the batching of the concrete [40]. Al-D, obtained from Aluminum Rolling Mill Factory in Ota, Ogun State, Nigeria, was dried and pulverized to reduce the particle size of the waste sample due to its effect on the structural properties and characteristic bond of admixtures [41].

**Table 1** Percentage nominal composition of LCS

| Element symbols | Mn | P | S | C | Fe |
|---|---|---|---|---|---|
| % Composition (LCS) | 0.8 | 0.04 | 0.05 | 0.16 | 98.95 |

### 2.2 Concrete Mix Design

The pulverized Al-D was added in wt% concentrations of 0%, 5%, 10%, 15%, 20% and 25% Al-D per the weight of cement used. The $H_2O$/cement ratio of 0.68 was applied based on the assertion of Kulakowski [42]. The concrete mix design is shown in Table 2.

### 2.3 Pore Electrolyte Extraction

The concrete pore electrolyte used in the analysis was extracted after 4 h from the onset of the hydration process of the cement in the fresh concrete mix. Further extraction was done manually. Additionally, load was applied on the specimen with the intention to promote confinement tension and expel the pore electrolyte [43]. The process of obtaining the pore electrolyte is extremely difficult; as a result, relatively small quantity of the pore electrolyte was obtainable to perform only a single set of experiments ($n=1$). The pH values of the concrete pore electrolytes shown in Table 3 were determined using Hanna calibration check pH meter HI223.

### 2.4 Electrochemical Tests

Potentiodynamic polarization test was conducted using a three-electrode system within a glass cell containing 200 mL of $H_2SO_4$/Al-D solution at specific Al-D concentrations with Digi-Ivy 2311 potentiostat connected to a computer. LCS mounted in hardened versocit acrylic resin with exposed surface area of 1.13 $cm^2$ is the working electrode, while platinum rod was used as the counter electrode and silver chloride electrode (3 molar concentrations

**Table 2** Mix design of concrete aggregates, cement Al-D and $H_2O$

| Replacement (%) | Coarse aggregate (kg) | Fine aggregate (kg) | Total aggregate weight (kg) | Cement (kg) | Al-D (kg) | $H_2O$/C ratio |
|---|---|---|---|---|---|---|
| 0 | 80 | 40 | 120 | 20 | 0 | 0.7 |
| 5 | 80 | 40 | 120 | 19 | 1 | 0.7 |
| 10 | 80 | 40 | 120 | 18 | 2 | 0.7 |
| 15 | 80 | 40 | 120 | 17 | 3 | 0.7 |
| 20 | 80 | 40 | 120 | 16 | 4 | 0.7 |
| 25 | 80 | 40 | 120 | 15 | 5 | 0.7 |

**Table 3** pH of concrete pore electrolyte with respect to Al-D concentration

| Al-D concentration (%) | 0 | 5 | 10 | 15 | 20 | 25 |
|---|---|---|---|---|---|---|
| pH value | 12.67 | 12.32 | 12.32 | 12.32 | 12.32 | 12.32 |

**Table 4** Results of calibration and hardware test

| RAM test | |
|---|---|
| Ok | |
| Current test results | |
| Sensitivity offset error (0%) | Gain error (0%) |
| Voltage test results | |
| Sensitivity offset error (0%) | Gain error (0%) |

at pH of 6.5) as the reference electrode. Anodic–cathodic polarization curves were plotted at scan rate of 0.0015 V/s between − 1.25 V and 1.75 V. The potential was stabilized for 10 min before polarization to attain quasi-steady state. Corrosion current density $C_{cd}$ (A/cm$^2$) and corrosion potential $C_p$ (V) were determined from the Tafel extrapolation method.

Corrosion rate $C_r$ (mm/year) was determined from the relationship below;

$$C_r = \frac{0.00327 \times C_{cd} \times E_{qw}}{D}. \quad (1)$$

$E_{qw}$ is the equivalent weight (g) of LCS, 0.00327 is a corrosion rate constant, and $D$ is the density (g). Experimental analysis was performed on the carbon steel in the pore electrolyte. The electrochemical system was checked for possible causes of systematic errors. The uncertainty of single measurement is limited by the precision and accuracy of the measuring instrument. As a result, calibration of the instrument and hardware test was performed with the results shown in Table 4. Test for reproducibility of consistent results was also performed.

Open circuit potential (OCP) measurement was taken at 0.1 V/s step potential for 5400 s to obtain information on active–passive behavior and electrochemical equilibrium of LCS without applied potentials. Images of the LCS surfaces (before corrosion and after corrosion from the concrete pore electrolyte at 5% and 25% Al-D) from optical microscopy were analyzed after polarization test with Omax trinocular metallurgical microscope through the aid of ToupCam analytical software.

## 3 Results and Discussion

### 3.1 Potentiodynamic Polarization Studies

Potentiodynamic polarization plots of the active–passive behavior of LCS in Al-D contaminated concrete pore electrolyte are shown in Fig. 1. Results of the polarization parameters are shown in Table 5. Comparison of the corrosion rate values (Table 5) shows Al-D has slight influence on the electrochemical behavior and corrosion resistance of LCS in the concrete pore electrolyte. At 0% Al-D concentration, LCS corrodes under applied potential, attaining a corrosion rate value of $3.00\times10^{-2}$ mm/year, which corresponds to a corrosion current density of $2.59\times10^{6}$ A/cm$^3$. The electrochemical mechanisms occurring within the concrete pore electrolyte are responsible for the corrosion of LCS. LCS oxidizes in the electrolyte losing electrons and releasing $Fe^{2+}$ cations which go into the electrolyte. This process gradually deteriorates the microstructural and mechanical properties of the steel according to Eq. 2. Cathodic reduction reactions also take place resulting in oxygen reduction and to a lesser extent hydrogen evolution reaction when the previously released electrons combine with $H_2O$ and $O_2$ in the concrete pore electrolyte according to Eq. 3. The corrosion product resulting from the combined electrochemical half-cell reactions is hydrated 2Fe(OH) known commonly as rust according to Eq. 4.

$$2Fe \rightarrow 2Fe^{2+} + 4e^{-}, \quad (2)$$

$$2H_2O + O_2 + 4e^{-} \rightarrow 4OH^{-}, \quad (3)$$

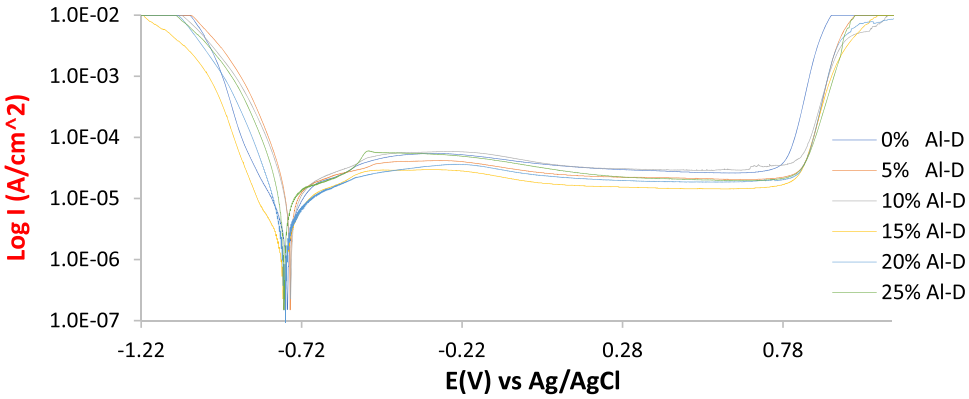


**Fig. 1** Potentiodynamic polarization plots for LCS corrosion in Al-D contaminated concrete pore solution at 0–25% Al-D concentration

**Table 5** Potentiodynamic polarization data for LCS corrosion in Al-D contaminated concrete pore solution at 0–25% Al-D concentration ($n=1$)

| Samples | Al-D concentration (%) | LCS $C_R$ (mm/year) | Corrosion current (A) | $C_{cd}$ (A/cm$^2$) | $C_P$ (V) | Polarization resistance, $R_p$(Ω) | Cathodic Tafel slope, $B_c$ (V/dec) | Anodic Tafel slope, $B_a$ (V/dec) |
|---|---|---|---|---|---|---|---|---|
| A | 0 | 3.00E−02 | 2.69E−06 | 2.59E−06 | − 0.746 | 4915.00 | − 9.412 | 5.096 |
| B | 5 | 3.41E−02 | 3.05E−06 | 2.94E−06 | − 0.802 | 8412.00 | − 13.440 | 2.434 |
| C | 10 | 4.02E−02 | 3.60E−06 | 3.47E−06 | − 0.754 | 7140.00 | − 12.910 | 3.352 |
| D | 15 | 5.02E−02 | 4.49E−06 | 4.33E−06 | − 0.774 | 5471.00 | − 13.030 | 3.249 |
| E | 20 | 5.04E−02 | 4.51E−06 | 4.34E−06 | − 0.770 | 5702.00 | − 11.493 | 4.265 |
| F | 25 | 8.39E−02 | 7.51E−06 | 7.23E−06 | − 0.775 | 7491.00 | − 13.120 | 4.973 |

$$2Fe^{2+} + 4OH^- \rightarrow 2Fe(OH). \quad (4)$$

An increase in Al-D concentration to 5% caused a mild increase in corrosion rate to $3.41 \times 10^{-2}$ mm/year which indicates that the characteristics of the oxide film formed with respect to Al-D differ. Beyond 5% Al-D, the corrosion rate of LCS increased with respect to Al-D concentration, attaining a peak value of $8.39 \times 10^{-2}$ mm/year at 25% Al-D concentration. The increase in corrosion rate occurs due to an increase in concentration of Al-D within the concrete pore electrolyte. Al being an amphoteric metal chemically reacts with the alkaline solutions prevalent in the concrete pore. According to Darwin et al. [44], the reaction results in the release of $H_2$ before possible passivation of Al. Auxiliary anions present within the concrete also influence the rate of Al reaction [45–49]. Generally, Al mainly occurs as aluminate complexes $[Al(OH)_4^-$ (aq)] in alkaline solutions. However, despite the incremental value of corrosion rate with respect to Al-D concentration, observation of the passivation behavior on the polarization plots shows Al-D could possibly have a positive influence of the electrochemical characteristics of LCS in concrete pore electrolyte. The shifts in corrosion potential value may not confirm this assertion. The corrosion potential value of $-0.746$ $V_{Ag/AgCl}$ (0% Al-D) shifts to $-0.775$ $V_{Ag/AgCl}$ at 25% Al-D concentration. The cathodic shift is due to destruction of the passive film resulting in selective deterioration of the steel. At the same time, it could be as a result of superficial electrochemical reactions occurring on the steel surface as a result of the presence of Al-D. Nevertheless, bridging the increase in corrosion rate values, cathodic shift in corrosion potential and extended passivation behavior of LCS in the concrete pore electrolyte with respect to Al-D, it can be surmised that the presence of Al-D improves the passivation behavior and briefly the corrosion resistance of LCS. However, upon collapse of the passive film corrosion accelerates on LCS.

## 3.2 Passivation and Pitting Corrosion Studies

Potentiodynamic polarization plots in Fig. 1 confirm the formation of protective oxide film formed on LCS surface during potential scanning. The plots display a passivated region where the corrosion current density is relatively low till the point where passivity transitions to transpassivity. This is the region where the passive protective film becomes unstable and rapidly collapses. During this period, metastable pitting corrosion dominates before stable pit propagation. During passivation, LCS is protected from corrosion due to the relative strength of the protective oxide on the steel surface. At the onset of pitting corrosion, the corrosion current density rises significantly leading to progressive breakdown

and collapse of the passive oxide film. The passivity of LCS is due to the high alkalinity of concrete pore electrolyte as earlier discussed [50, 51]. Potentiostatic data from LCS polarization plots are shown in Table 6, while Fig. 2 is a close-up view of region where localized corrosion reaction sets in. Observation of the table shows the presence of Al-D slightly improves the passivation and localized corrosion resistance properties of LCS. At 0% Al-D, the passivation range value is 1.456 V, while in the presence of varying concentration of Al-D the high and low points of the passivation range are 1.555 V and 1.534 V. The potential before the onset of localized corrosion reaction phenomena, i.e., metastable pitting activity, also shows the influence of Al-D on the electrochemical reaction processes. Al-D extends the potential at which the passive oxide begins to breakdown from 0.71 V at 0% Al-D to potentials between 0.77 and 0.78 V. The plot in Fig. 2 shows the metastable pitting activity of LCS at 0% Al-D occurs at higher corrosion current density and lower corrosion potential. Within this region, the rate of repassivation is slower and eventually overwhelmed by the film breakdown mechanism [52]. The degree of electrochemical activity at this concentration (0% Al-D) is much higher resulting in accelerated corrosion compared to the plots at varying concentrations of Al-D. Aggressive anions within the concrete pore electrolyte displace the anions responsible for passivation of LCS surface [53].

### 3.3 Open Circuit Corrosion Potential Measurement

LCS was exposed to concrete pore electrolytes at 0%, 5% and 25% Al-D and the corrosion potential was measured with respect to exposure time. Generally similar OCP plot is displayed in Fig. 3 by LCS in the electrolytes studied signifying similar active–passive corrosion thermodynamic behavior of the steel though differences do exist which helps to understand the nature of the electrochemical reactions occurring at rest potential. The corrosion potential values of LCS at 0% Al-D briefly decreased for the first 17 s of exposure from $-0.506$ $V_{Ag/AgCl}$ (0 s) to $-0.518$ $V_{Ag/AgCl}$, after which a steep increase in corrosion potential occurred to $-0.399$ $V_{Ag/AgCl}$ at 300 s. Beyond 300 s, the rate of increase in corrosion potential reduced substantially causing a parabolic curvature until 1800 s at $-0.209$ $V_{Ag/AgCl}$ where quasi-steady equilibrium state was achieved due to the spontaneous growth of the protective passive oxide on LCS surface. The interaction of adsorbed $O_2$ with the ionized LCS surface is responsible for the formation of the oxide film. The corrosion potential of LCS at 0% Al-D peaks at $-0.164$ $V_{Ag/AgCl}$ which greatly differs from its value at 0 s. This phenomenon increases the activation energy for the surface deterioration of LCS as a result the leaching of LCS cations away from the steel surface is effectively controlled. At 0 s the corrosion potential of LCS at 5% and 25% Al-D initiated at values of $-0.667$ $V_{Ag/AgCl}$ and $-0.793$ $V_{Ag/AgCl}$ which

**Table 6** Potentiostatic data for localized corrosion evaluation for LCS in concrete pore electrolyte at 0–25% Al-D concentration ($n=1$)

| Samples | Al-D concentration (%) | Corrosion potential (V) | Potential before transpassivity (V) | Current before transpassivity (A) | Passivation range (V) |
|---|---|---|---|---|---|
| A | 0 | −0.746 | 0.71 | 2.74E−05 | 1.456 |
| B | 5 | −0.762 | 0.78 | 2.22E−05 | 1.542 |
| C | 10 | −0.754 | 0.78 | 3.58E−05 | 1.534 |
| D | 15 | −0.774 | 0.77 | 1.65E−05 | 1.544 |
| E | 20 | −0.770 | 0.77 | 1.98E−05 | 1.540 |
| F | 25 | −0.775 | 0.78 | 2.13E−05 | 1.555 |

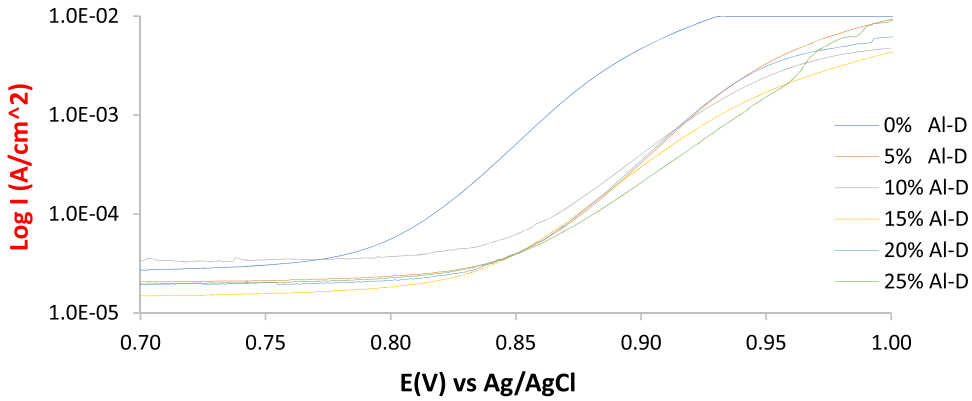


**Fig. 2** Polarization plot of the pitting region of LCS corrosion during potential scanning in concrete pore solution at 0–25% Al-D concentration

are significantly more electronegative than the corrosion potential of LCS at 0% Al-D. As earlier mentioned, similar OCP plot was displayed by LCS at 5% and 25% Al-D compared to the plot at 0% Al-D. The lower pH values of the concrete pore electrolyte at 5% and 25% Al-D mean the hydration, and diffusion of LCS cations in the concrete pore electrolyte is more prevalent. However, at 4900 s the OCP plot of LCS at 5% Al-D links with the plot at 0% Al-D ($-0.175$ $V_{Ag/AgCl}$) to peak at $-0.166$ V at 5400 s while the plot 25% Al-D peaked at $-0.187$ $V_{Ag/AgCl}$ (5400 s). This shows that Al-D has negligible effect to the passivation properties of LCS in concrete pore electrolyte without applied potential.

### 3.4 Morphological Studies

Optical images of LCS morphology (mag. ×10 and ×40) before corrosion and after corrosion from the concrete pore electrolyte at 0%, 5% and 25% Al-D are shown in Figs. 4, 5, 6 and 7. Severe morphological deterioration in the form of corrosion pits of different sizes occurred in Fig. 5 due to the electrochemical action of corrosive anions present within the electrolyte. Figure 6 shows the presence of fewer,

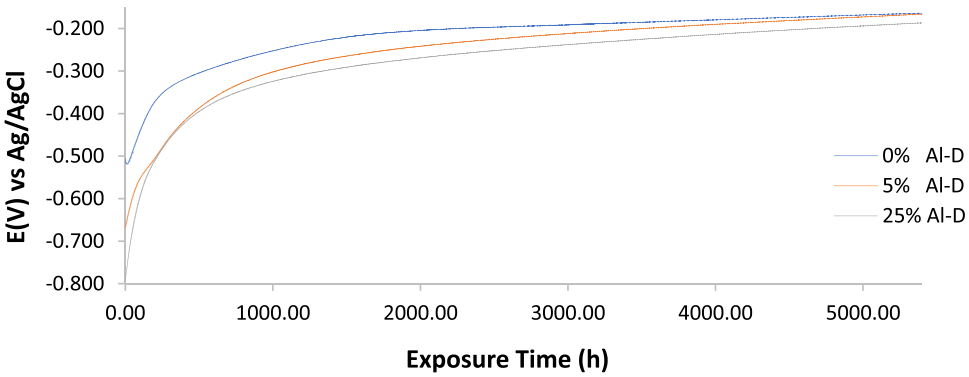


**Fig. 3** Variation in OCP plot of LCS (0%, 5% and 25% Al-D) versus exposure time

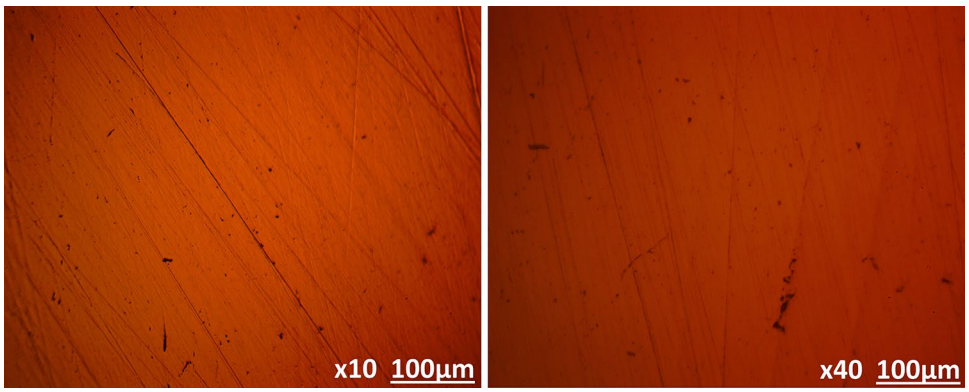


**Fig. 4** Optical microscopy images of LCS morphology before corrosion

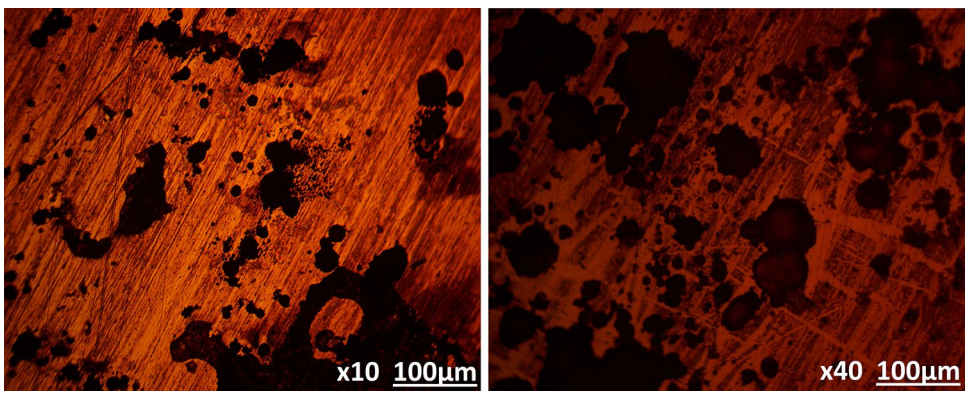


**Fig. 5** Optical microscopy images of LCS morphology after corrosion from concrete pore electrolyte/0% Al-D

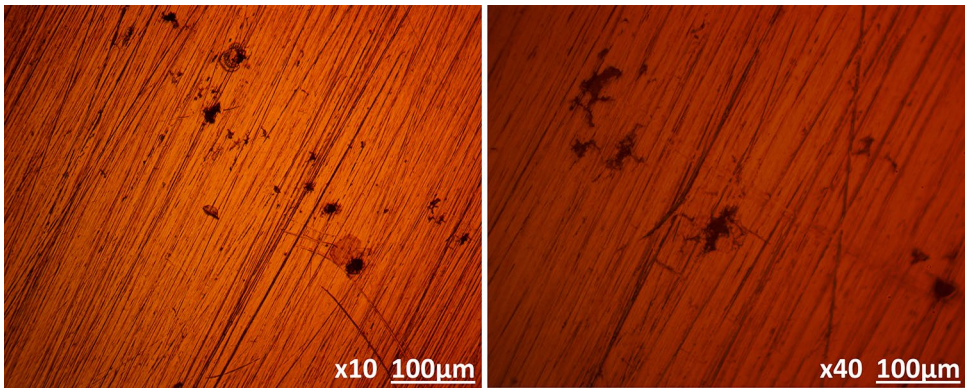


**Fig. 6** Optical microscopy images of LCS morphology after corrosion from concrete pore electrolyte/5% Al-D

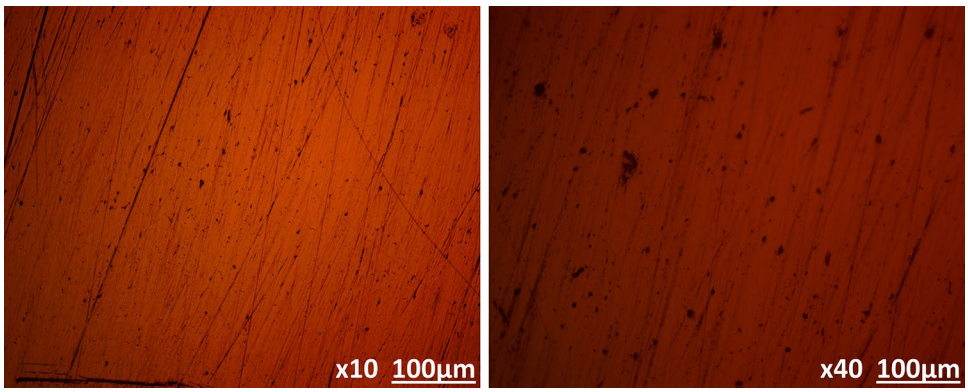


**Fig. 7** Optical microscopy images of LCS morphology after corrosion from concrete pore electrolyte/25% Al-D

smaller and comparatively shallower corrosion pits, while in Fig. 7 numerous microscopic corrosion pits are visible. This observation contrasts the corrosion rate results in Table 5. LCS at 0% Al-D had the lowest corrosion rate from potentiodynamic polarization test and yet has the most severe morphological deterioration, while Fig. 7 has the highest corrosion rate value with the mildest morphological deterioration. Comparing the optical images with the results from passivation and pitting corrosion evaluation, it is clearly visible that Al-D improves the localized corrosion resistance of LCS despite minimal increase in general corrosion rate. At 25% Al-D, the effect of the corrosive anions on the pitting corrosion resistance of LCS has been significantly curtailed. Under the influence of applied potential, the passive film will eventually breakdown; however, the small microscopic pits show the breakdown likely occurred at sites or regions where microscopic impurities are prevalent.

## 4 Conclusion

Al-D in concrete enhanced the passivation and pitting corrosion resistance of carbon steel in concrete pore electrolyte. The passivation range of the polarization plots and pitting potential increased with an increase in Al-D concentration. The morphology of the carbon steel in the concrete pore without Al-D showed the presence of localized corrosion damage in addition to a severely pitted surface. This contrasts the morphology of the steel from the pore electrolyte at specific Al-D concentration which showed very limited surface deterioration.

**Acknowledgements** The authors acknowledge Covenant University Ota, Ogun State, Nigeria, for the sponsorship and provision of research facilities for this project.

## Compliance with Ethical Standards

**Conflict of interest** The authors declare that they have no conflict of interest.

## References

1. Ahmad S (2003) Reinforcement corrosion in concrete structures, its monitoring and service life prediction—a review. Cem Concr Compos 25(4–5):459–471
2. Biezma MV, San JR, Cristobal (2005) Methodology to study cost of corrosion. Corros Eng Sci Techno l40(4):344–352
3. Thangavel K (2004) The threshold limit for chloride corrosion of reinforced concrete. Corros Rev 22(1):55–70

4. Zheng H, Li W, Ma F, Kong Q (2012) The effect of a surface-applied corrosion inhibitor on the durability of concrete. Constr Build Mater 37:36–40
5. Bastidas DM, Criado M, Fajardo S, La Iglesia A, Bastidas JM (2015) Corrosion inhibition mechanism of phosphates for early-age reinforced mortar in the presence of chlorides. Cem Concr Compos 61:1–6
6. Conciatori F, Laferrier E, Brruhwiler (2010) Comprehensive modeling of chloride ion and water ingress into concrete considering thermal and carbonation state for real climate. Cem Concr Res 40(1):109–118
7. Etteyeb N, Novoa XR (2016) Inhibition effect of some trees cultivated in arid regions against the corrosion of steel reinforcement in alkaline chloride solution. Corros Sci 112:471–482
8. Loto CA, Joseph OO, Loto RT (2013) Inhibition effect of *Vernonia amygdalina* extract on the corrosion of mild steel reinforcement in concrete in 0.2 M $H_2SO_4$ environment. Eur J Environ Civ Eng 17(10):1026–1038
9. Loto RT, Loto CA, Fedotova T (2014) Electrochemical studies of mild steel corrosion inhibition in sulfuric acid chloride by aniline. Res Chem Intermed 40(4):1501–1516
10. Loto CA, Loto RT (2013) Effect of dextrin and thiourea additives on the zinc electroplated mild steel in acid chloride solution. Int J Electrochem Sci 8(12):12434–12450
11. William HH (2014) Analytical evaluation of time-to-corrosion for chloride-exposed reinforced concrete with an admixed corrosion inhibitor: Part 1—no inhibitor egress. Corrosion 70(1):48–55
12. Tang SW, Yao Y, Andrade C, Li ZR (2015) Recent durability studies on concrete structure. Cem Concr Res 78:143–154
13. Ryu H, Singh JK, Lee H-S, Ismail MA, Park WJ (2017) Effect of $LiNO_2$ inhibitor on corrosion characteristics of steel rebar in saturated $Ca(OH)_2$ solution containing NaCl: an electrochemical study. Constr Build Mater 133:387–396
14. Moreno M, Morris W, Alvarez MG, Duffo GS (2004) Corrosion of reinforcing steel in simulated concrete pore solutions: effect of carbonation and chloride content. Corros Sci 46(11):2681–2699
15. Kumar V (1998) Protection of steel reinforcement for concrete: a review. Corros Rev 16(4):317–358
16. Maslehuddin M, Al-Zahrani MM, Ibrahim M, Al-Mehthel MH, Al-Idi SH (2007) Effect of chloride concentration in soil on reinforcement corrosion. Constr Build Mater 21:1825–1832
17. Hussain RR, Shuraim AB, Alhozaimy AMA (2015) Investigation for the impact of nature of coarse aggregate on the passive layer formation and corresponding corrosion of reinforcement bars in high performance concrete. Constr Build Mater 100:52–62
18. Wasim M, Hussain RR (2015) Passive film formation and corrosion initiation in lightweight concrete structures as compared to self-compacting and ordinary concrete structures at elevated temperature in chloride rich marine environment. Constr Build Mater 78:144–152
19. Holloway L, Nairn K, Forsyth M (2004) Concentration monitoring and performance of a migratory corrosion inhibitor in steel-reinforced concrete. Cem Concr Res 34(8):1435–1440
20. Ann KY, Song HW (2007) Chloride threshold level for corrosion of steel in concrete. Corros Sci 49:4113–4133
21. Mennucci MM, Banczek EP, Rodrigues PRP, Costa I (2009) Evaluation of benzotriazole as corrosion inhibitor for carbon steel in simulated pore solution. Cem Concr Compos 31(6):418–424
22. Huet B, L'Hostis V, Miserque F, Idrissi H (2005) Electrochemical behavior of mild steel in concrete: influence of pH and carbonate content of concrete pore solution. Electrochem Acta 51:172–180
23. Eichler T, Burkert A, Beck M (2007) Electrochemical noise measurements on unalloyed steel in chloride-containing alkaline environment. Mater Corros 58:961–969
24. Wang Y, Cheng G, Wu W, Qiao Q, Li Y, Li X (2015) Effect of pH and chloride on the micro-mechanism of pitting corrosion for high strength pipeline steel in aerated NaCl solutions. Appl Surf Sci 349:746–756
25. Perez N (2016) Electrochemistry and corrosion science, 2nd edn. Springer, Boston. https://doi.org/10.1007/978-3-319-24847-9
26. Shi J, Sun W, Jiang J, Zhang Y (2016) Influence of chloride concentration and pre-passivation on the pitting corrosion resistance of low-alloy reinforcing steel in simulated concrete pore solution. Constr Build Mater 111:805–813
27. Luo H, Su H, Dong C, Xiao K, Li X (2015) Electrochemical and passivation behavior investigation of ferritic stainless steel in alkaline environment. Constr Build Mater 96:502–507
28. Taveira LV, Montemor MF, Belo MDC, Ferreira MG, Dick LFP (2010) Influence of incorporated Mo and Nb on the Mott–Schottky behavior of anodic films formed on AISI 304L. Corros Sci 52:2813–2818
29. Marcotte TD (2001) Characterization of chloride-induced corrosion products that forms in steel reinforced cementitious materials. PhD Thesis, University of Waterloo
30. Kulik GJ, Daley JC (1990) Aluminum dross processing in the 90's. In: 2nd International symposium—recycling of metals and engineered materials. TMS-AIME, Warrendale
31. Gwinner DS (1996) Environmental issues in the aluminum reclamation industry. In: IX international seminar on aluminum recycling discusses sustainability, São Paulo, SP, Brazil, p 40–51
32. Peterson RD, Newton L (2002) Review of aluminum dross processing, light metals. TMS-AIME, Warrendale
33. Busari A, Akinmusuru J, Dahunsi B (2017) Mechanical properties of dehydroxylated kaolinitic clay in self-compacting concrete for pavement construction. Silicon. https://doi.org/10.1007/s12633-017-9654-6
34. Puertas F, Blanco-Varela MT, Vazquez T (1999) Behaviour of cement mortars containing an industrial waste from aluminum refining. Cem Concr Res 29:1673–1680
35. Ewais EMM, Khalil NM, Amin MS, Ahmed YMA, Barakat MA (2009) Utilization of aluminum sludge and aluminum slag (dross) for the manufacture of calcium aluminate cement. Ceram Int 35(8):3381–3388
36. Elinwa AU, Mbadike E (2011) The use of aluminum waste for concrete production. J Asian Archit Build Eng 10(1):217–220
37. Arimanwa JI, Onwuka DO, Arimanwa MC, Onwuka US (2012) Prediction of the compressive strength of aluminum waste–cement concrete using Scheffe's theory. J Mater Civil Eng 24(2):177–183
38. NIS 444-1:2003 composition, specification and conformity criteria for common cements. Standards Organization of Nigeria
39. NIS 11 (1974) Specification for ordinary Portland cement. Standards Organization of Nigeria
40. Mindess S, Young JF, Darwin D (2003) Concrete, 2nd edn. Pearson Education, Upper Saddle River
41. Ayobami Busari A, Akinmusuru J, Dahunsi B (2017) Mechanical properties of dehydroxylated kaolinitic clay in self-compacting concrete for pavement construction. Silicon. https://doi.org/10.1007/s12633-017-9654-6
42. Kulakowski MP (2002) Contribution to the study of carbonation in concretes and composite mortars with active silica addition. Doctoral Thesis. Federal University of Rio Grande do Sul, Porto Alegre
43. Ortolan VK, Mancio M, Tutikian BF (2016) Evaluation of the influence of the pH of concrete pore solution on the corrosion resistance of steel reinforcement. J Build Rehabil1:10. https://doi.org/10.1007/s41024-016-0011-8
44. Darwin D, Browning JA, O'Reilly M, Xing L, Ji J (2009) Critical chloride corrosion threshold of galvanized reinforcing bars. ACI Mater J 106(2):176–183
45. Moragues A, Macias A, Andrade C (1987) Equilibria of the chemical composition of the concrete pore solution. Part I: comparative

study of synthetic and extracted solutions. Cem Concr Res 17(2):173–182
46. Saremi M, Mahallati E (2002) A study on chloride-induced depassivation of mild steel in simulated concrete pore solution. Cem Concr Res 32:1915–1921
47. Andersson K, Allard B, Bengtsson M, Magnusson B (1989) Chemical composition of cement pore solutions. Cem Concr Res 19:327–332
48. Blanco G, Bautista A, Takenouti H (2006) EIS study of passivation of austenitic and duplex stainless steels reinforcements in simulated pore solutions. Cem Concr Compos 28(3):212–219
49. Monticelli C, Frignani A, Trabanelli G (2000) A study on corrosion inhibitors for concrete application. Cem Concr Res 30:635–642
50. Ormellese M, Berra M, Bolzoni F, Pastore T (2006) Corrosion inhibitors for chlorides induced corrosion in reinforced concrete structures. Cem Concr Res 36(3):536–547
51. Morris W, Vico A, Vazquez M, DeSanchez S (2002) Corrosion of reinforcing steel evaluated by means of concrete resistivity measurements. Corros Sci 44(1):81–99
52. Balytes OI, Krokhrnal'nylOO (1999) Pitting corrosion of 12Kh 18AG 18Sh steel in chloride solutions. Mater Sci 35(3):389–394
53. Abd El-Haleem SM, Abd El-Wanees S (2011) Chloride induced pitting corrosion of nickel in alkaline solutions and its inhibition by organic amines. Mater Chem Phys 128(3):418–426